Experimental Brain Research (2019) 237:2367–2385
https://doi.org/10.1007/s00221-019-05595-y

RESEARCH ARTICLE

Differential functional patterns of the human posterior cingulate cortex during activation and deactivation: a meta-analytic connectivity model

Jessica N. Busler[1,2,3,4] · **Julio A. Yanes**[1,2,3,4] · **Ryan T. Bird**[1,2,3,4] · **Meredith A. Reid**[1,2,3,4] · **Jennifer L. Robinson**[1,2,3,4]

Received: 6 August 2018 / Accepted: 2 July 2019 / Published online: 10 July 2019

Abstract

The posterior cingulate cortex (PCC) has been implicated in a host of cognitive and behavioral processes in addition to serving as a central hub in the default mode network (DMN). Moreover, the PCC has been shown to be involved in a range of psychiatric and neurological disorders. However, very little is known about the specific activated/deactivated functional profiles of the PCC. Here, we employed a dual analytic approach using robust quantitative meta-analytical connectivity modeling (MACM) and ultra-high field, high resolution resting state functional magnetic resonance imaging (rs-fMRI) to identify state-specific functional activity patterns of the human PCC. The MACM results provided evidence for regions of convergence for PCC co-activation and co-deactivation (i.e., left medial frontal gyrus, left amygdala, and left anterior cingulate) as well as regions of divergence specific to either PCC activation (i.e., bilateral inferior frontal gyri) or PCC deactivation (i.e., left parahippocampal gyrus). In addition, exploratory MACMs on dorsal and ventral subregions of the PCC revealed differential functional activity patterns such as greater co-activation of the right PCC and left inferior parietal lobule with the dorsal PCC and greater co-activation of right precuneus with the ventral PCC. Resting state connectivity analyses showed widespread connectivity similar to that of the PCC co-activation-based MACM, but also demonstrated additional regions of activity, including bilateral superior parietal regions and right superior temporal regions. These analyses highlight the diverse neurofunctional repertoire of the human PCC, provide additional insight into its dynamic functional activity patterns as it switches between activated and deactivated states, and elucidates the cognitive processes that may be implicated in clinical populations.

Keywords Brain · Neuroimaging · Magnetic resonance imaging · Activation analysis · Attention

Introduction

In addition to serving as a central hub in the default mode network (DMN), the posterior cingulate cortex (PCC) has been implicated in a host of cognitive and behavioral processes, rendering it one of the most dynamic structures in the human brain. Despite our understanding of the functional role of the PCC via specific task designs and analytical approaches [i.e., region-of-interest (ROI) analyses], more can be gleaned about this key structure by combining techniques that investigate different states of the PCC, such as activation, deactivation, and resting state. Here, we extend the literature by employing a complementary analytic approach using robust quantitative meta-analytic techniques along with ultra-high field, high resolution resting state functional magnetic resonance imaging (rs-fMRI).

Electronic supplementary material The online version of this article (https://doi.org/10.1007/s00221-019-05595-y) contains supplementary material, which is available to authorized users.

✉ Jessica N. Busler
jbusler@auburn.edu

[1] Department of Psychology, Auburn University, 226 Thach Hall, Auburn, AL 36849, USA

[2] Auburn University Magnetic Resonance Imaging Research Center, 560 Devall Drive, Auburn, AL 36849, USA

[3] Alabama Advanced Imaging Consortium, Auburn University, 560 Devall Road, Auburn, AL 36849, USA

[4] Center for Neuroscience Initiative, Auburn University, Auburn, AL 36849, USA

Perhaps the PCC's most well-defined role is that of a "cortical hub", due to evidence suggesting that the PCC may serve a vital role within multiple functional neural networks as well as its membership in the "rich club" of the human connectome (Lord et al. 2017; van den Heuvel and Sporns 2011). As noted previously, the PCC serves as an anchor to the DMN, a collection of brain regions characterized by blood-oxygen level dependent (BOLD) signal timeseries correlations during rest (i.e., task-negative) conditions and anticorrelations to regions comprising the task-positive network (Yu et al. 2011). In addition, the PCC is the only DMN node that interacts with all but one of the other DMN nodes, the right medial temporal lobe (MTL) (Leech et al. 2012), underscoring this structure's influence within the DMN. Furthermore, Fransson and Marrelec (2008) demonstrated extensive functional connectivity of the PCC throughout the brain, including connectivity to structures involved in cognitive and affective processing [i.e., dorsal and ventral medial prefrontal cortices (dmPFC, vmPFC, respectively), left medial temporal lobe (lMTL)], as well as sensory processing [i.e., precuneus, bilateral temporal cortices (lTC, rTC), bilateral inferior parietal lobe (lIPL, rIPL)] emphasizing its functional versatility and importance. Given its role in the DMN, the PCC has been noted to be deactivated during cognitive tasks involving externally directed thought and attention (Singh and Fawcett 2008) and active in tasks involving internally directed thought, such as memory recollection or daydreaming (Buckner et al. 2008). In addition, connections to frontoparietal attention networks have been linked to regions of deactivation within the PCC (Leech et al. 2012). This suggests the PCC may deactivate or activate for reasons unrelated to the PCC's connection to the DMN, a part of the PCC's neurofunctional repertoire that has received little attention.

The PCC and precuneus have been shown to be two of the most metabolically active regions of the brain both at rest and during cognitive tasks (Raichle et al. 2001), further suggesting the structure as being highly dynamic in function not just within the realm of DMN. For example, the PCC operates in other neural networks such as the fronto-parietal control, dorsal attention, salience, sensorimotor networks (Leech and Sharp 2014) and parietal memory network (Gilmore et al. 2015). Additionally, the PCC has demonstrated sensitivity to sleep, as evidence suggests that its neurofunctional profile (i.e., connectivity between the PCC and other regions of the brain) changes depending on the amount and quality of sleep (Robinson et al. 2018; Sämann et al. 2011). Furthermore, the PCC is activated across a diverse range of cognitive and behavioral tasks related to emotional stimulus processing (Maddock et al. 2003), autobiographical information processing (Maddock et al. 2001), consciousness/self-reflection (Vogt and Laureys 2005), and general monitoring of internal and external information (Raichle et al. 2001). In addition to the role the PCC plays in healthy brain functioning, structural, functional, and/or connectivity abnormalities of the PCC have been noted in a wide range of conditions including neurological and psychiatric conditions (Buckner et al. 2008; Zhu et al. 2012; Vogt and Laureys 2005; Miller et al. 2015) such as attention deficit hyperactivity disorder (Nakao et al. 2011), amnestic type mild cognitive impairment (Bai et al. 2009), autism spectrum disorder (Cherkassky et al. 2006), and schizophrenia (Liang et al. 2006). Together, these data suggest that the PCC may have unique functional patterns compared to other regions of the brain, and likely has a strong evolutionary purpose given its extensive involvement across cognitive, emotion, attentional, neurological, and psychiatric states.

Functional activity patterns of the PCC have, at least in part, been attributed to dorsal and ventral subregions of the PCC (Cha et al. 2017; Vogt et al. 2006; Yu et al. 2011). Differences in functional activity between dorsal and ventral regions of the PCC are suggested to be a result of local connectivity differences (Cha et al. 2017). Specifically, the dorsal PCC (dPCC) has been implicated to be functionally specialized in spatial orientation, and the ventral PCC (vPCC) in self-relevant information processing (Vogt et al. 2006). In addition, the vPCC has been shown to be functionally connected to the ventromedial prefrontal cortex and middle left inferior parietal cortex and associated with facial appraisal and language tasks (Bzdok et al. 2015). The dPCC has been shown to be functionally connected to the dorsomedial prefrontal cortex as well as anterior and posterior inferior parietal cortex regions and associated with delay discounting and subjective value tasks (Acikalin et al. 2017; Bzdok et al. 2015). Although functional specializations for the dPCC and vPCC exist, both regions have been shown to be positively correlated with the DMN (Yu et al. 2011).

Despite established functional specialization of subregions within the PCC, very little is known about how activated and deactivated functional profiles of the PCC, and those of its dorsal and ventral subregions, differ. This gap in knowledge is, in part, related to biases in the fMRI literature towards studies reporting activation coordinates. The lack of attention to deactivations in the PCC, and in general, underscores the need for data-driven approaches to understanding PCC function that incorporates both co-activation and co-deactivation. Thus, a goal of the current paper is to contribute to this gap in knowledge regarding signal decreases in the brain, by capitalizing on meta-analytic techniques to derive a PCC task-based co-deactivation functional profile and to then compare that profile to a task-based co-activation profile as well as a task-independent resting state profile. In addition, considering dPCC and vPCC subregions, we sought to conduct exploratory investigations of the co-activation and co-deactivation profiles of dorsal and ventral subregions of

the PCC. Because the PCC is a high-degree node in the "rich club" indicating that it plays a key role in global information integration and that structural, functional, and metabolic changes in the PCC are linked to neuropathology, co-activation, co-deactivation, and resting state functional profiles would be expected to differ. To assess neurofunctional differences among PCC activation, deactivation, and resting state, we employed a multi-method approach by combining robust meta-analytic techniques with ultra-high field [i.e., 7 Tesla (7T)], submillimeter rs-fMRI. Ultra-high-field scanners have been shown to have greater signal-to-noise ratio, provide better measures of brain connectivity (Nowogrodzki 2018), and are becoming increasingly incorporated in academic and clinical research. Furthermore, functional connectivity measurements at 7T compared to 3T show improved spatial specificity in rs-fMRI for delineating the DMN and sensorimotor networks (SMN; Hale et al. 2010). Given these advantages, the current work provided characterization of PCC connectivity using ultra-high field high-resolution data. In addition, to determine psychological phenomena associated with specific activation profiles, we conducted data-driven regional decoding assessments using taxonomic meta-data terms including behavioral domains and paradigm classes. To our knowledge, the function of the PCC has yet to be explored by comparing and contrasting the different states of activity (i.e., activated, deactivated, resting). Improving our understanding of PCC function in this manner may elucidate models of disease by contributing to our understanding of functional changes as the PCC dynamically switches between activated, deactivated, and resting states.

Methods

Overview

We examined functional differences between activation and deactivation of the human PCC. To do this, we leveraged the organization of the BrainMap® database (Fox et al. 2005; Laird et al. 2005a) and the BrainMap® utility, Sleuth, to conduct meta-analytic connectivity modeling (MACM), a quantitative method for assessing patterns of concurrent neural activity (Robinson et al. 2009). This provided an initial model of task-based co-activation and co-deactivation patterns utilizing decades worth of neuroimaging data collected across various behavioral domains. We also performed submillimeter, ultra-high field (7T) rs-fMRI in a sample of healthy individuals for comparison and validation of more subtle effects that may be seen with high-field imaging.

ROI construction

We defined the PCC ROI using the Harvard–Oxford Structural Probability Atlas (thresholded at 50% probability, Fig. 1) distributed with FSL neuroimaging analysis software (http://fsl.fmrib.ox.ac.uk/fsl/fslwiki/Atlases). The mean probability for the PCC was over 70% ($M \pm SD$: 70.53 ± 15.01) and the centroid (located at MNI coordinate 0, – 35, 33) was 96%. The total volume for the PCC was 10,816 voxels. Centroid, average threshold, and volume statistics were gathered using Mango's ROI analysis and histogram capabilities as well as FSL's 'fslstats' utility (http://ric.uthscsa.edu/mango, http://fsl.fmrib.ox.ac.uk/fsl/fslwiki/Fslutils?highlight=%28fslstats%29). Prior to use in the following meta-analyses, the PCC ROI was binarized using FSL's 'fslstats'.

Dorsal–ventral PCC

Because previous studies have reported neurofunctional differences between the dorsal and ventral portions of the PCC (Bzdok et al. 2015; Leech et al. 2011), we created dorsal/ventral PCC ROIs for use in exploratory meta-analyses. Here we defined the dPCC ROI as the region of the posterior cingulate associated with areas 23c, 23d, d23, and adjacent area 31 and the vPCC ROI as the portion of the PCC associated with v23 and caudal area 31, in line with previous research (Vogt et al. 2006; Yu et al. 2011). We used FSLeyes (https://fsl.fmrib.ox.ac.uk/fsl/fslwiki/FSLeyes) to construct the dPCC and vPCC ROIs. Within FSLeyes, we used the atlas panel to search for "posterior cingulate". From the search results we selected bilateral regions of the posterior cingulate specific to Brodmann Areas (BAs) 23 and 31 and exported the overlays. These overlays were then opened in Mango and assembled into a single ROI. To differentiate the dPCC and vPCC subregions, we divided the PCC ROI, inclusive of BAs 23 and 31, along the ventral branch of the splenial sulcus, which has been previously established as the cytological and functional border of the dPCC and vPCC regions (Yu et al. 2011; Fig. 1).

The PCC, dPCC, and vPCC ROIs were exported for use in the following meta-analytic procedures.

BrainMap® meta-analysis methods

Six separate meta-analyses were preformed, one meta-analysis for studies reporting co-activation with the PCC and a separate meta-analysis reporting studies associated with co-deactivations of the PCC as well as separate co-activation and co-deactivation meta-analyses for the dPCC and vPCC subregions. The PCC ROI was used to query the database to determine those brain regions which co-activate or co-deactivate with the PCC across included studies (Fox et al. 2005;

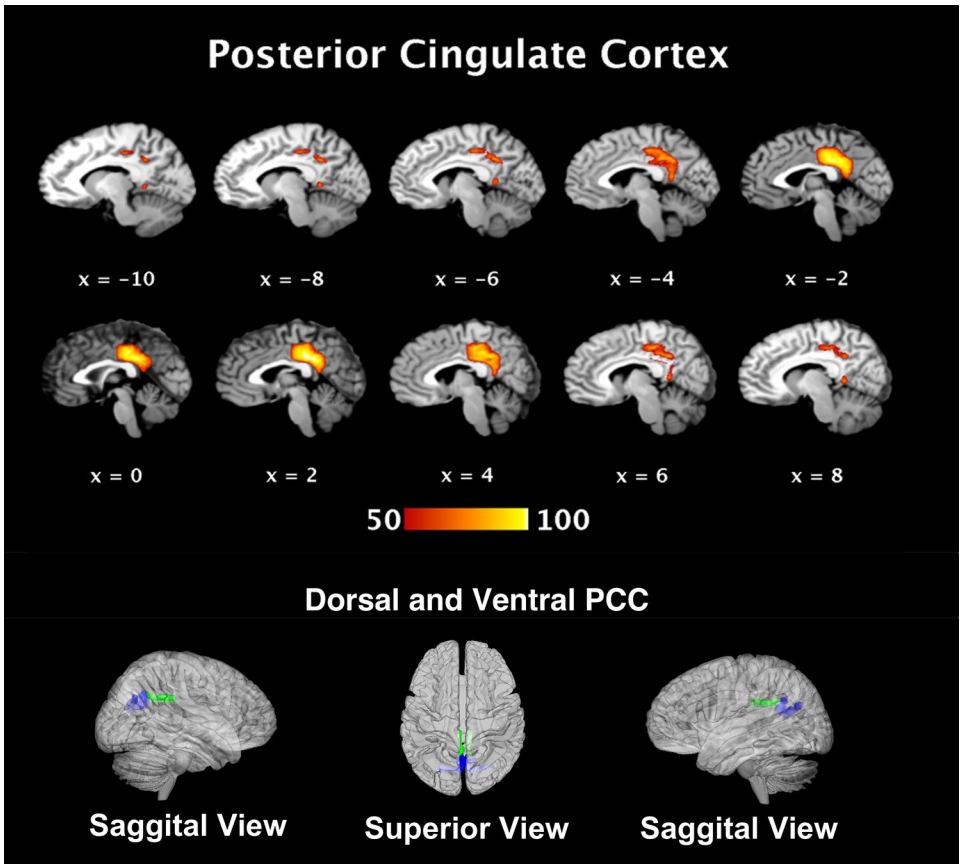

Fig. 1 PCC ROI mosaic with dorsal and ventral 3D ROIs in sagittal and superior renderings. The color bar represents the probability threshold across all voxels of the PCC ROI

Laird et al. 2005b) using Sleuth Version 2.4 (http://BrainMap.org/sleuth/), with the following criteria applied: (1) Locations → MNI Image → "PCC ROI", (2) Experiments → Context → Normal Mapping, (3) Experiments → Activation → Activations Only (or Deactivations Only). Whole-brain coordinates of co-activations (or co-deactivations) from the isolated contrasts were then downloaded (activations = 294 papers, 5720 locations, 393 experiments, 864 conditions, 5103 subjects; deactivations = 53 papers, 986 locations, 78 experiments, 156 conditions, 793 subjects). At the time of the search, the BrainMap® functional database contained 2994 papers, 108 paradigm classes, 62,902 subjects, 14,720 experiments, and 115,364 locations. Experiments for the PCC meta-analysis originated from multiple behavioral domains including Action, Cognition, Emotion, Interoception, and Perception with Emotion representing the majority of the studies followed by (in order) Perception, Action, Cognition, and Interoception for PCC co-activations. For PCC co-deactivations, the majority of the studies came from the Cognition behavioral domain followed by (in order) Perception, Action, Emotion, and Interoception. Behavioral domains and sub-domains were operationally defined by the BrainMap® lexicon (www.brainmap.org/taxonomy/). For example, the Action behavioral domain is defined as the mental faculty associated with overt movements of the body. Cognition is defined as the mental process of knowing, including the integration of awareness, perception, reasoning, and judgment. Emotion is defined as the mental faculty of experiencing an affective state of consciousness such as joy, sorrow, fear, hate, etc. Interoception is defined as the mental faculty associated with sensitivity to stimuli originating inside the body. Last, Perception is defined as the mental faculty of apprehending knowledge by means of the senses. Each behavioral domain has a number of sub-domains to further specify the function (for the complete listing see www.brainmap.org/taxonomy/). Articles are entered into the BrainMap® database through the Scribe application (http://brainmap.org/scribe/) primarily through a team of trained staff, but can also be entered by individual investigators. Meta-data from each article is entered and coded according to the BrainMap Lexicon (www.brainmap.org/scribe/BrainMapLex.xls) which includes citation, subject, and experiment information as well as paradigm class and behavioral domain. All papers entered are checked for accuracy before being added to the database.

Dorsal–ventral subdivision

Using the same procedure as above, whole-brain coordinates for co-activations and co-deactivations were

downloaded for the dPCC (activations = 41 papers, 2523 locations, 228 experiments, 150 conditions, 837 subjects; deactivations = 7 papers, 370 locations, 42 experiments, 33 conditions, 146 subjects) and vPCC (activations = 65 papers, 4879 locations, 457 experiments, 245 conditions, 1365 subjects; deactivations = 20 papers, 1779 locations, 187 experiments, 91 conditions, 293 subjects) ROIs. For both the dPCC and vPCC co-activation MACMs, the majority of the studies came from the Cognition behavioral domain followed by Emotion, Perception, Action, and Interoception. For dPCC co-deactivations, the majority of the studies came from the Cognition behavioral domain followed by Perception, Interoception, and Emotion. For vPCC co-deactivations, the majority of the studies came from the Cognition behavioral domain followed by Perception, Interoception, Action, and Emotion.

Activation likelihood estimation Using GingerALE 2.3.6 (http://BrainMap.org/ale/), (Eickhoff et al. 2009; Eickhoff et al. 2012; Turkeltaub et al. 2012), we performed random-effects activation likelihood estimation (ALE) meta-analyses (Laird et al. 2005a; Turkeltaub et al. 2012) on sets of coordinates identified as co-activated with the PCC and co-deactivated with the PCC to identify regions of convergence and likewise for the dPCC and vPCC. ALE capitalizes on the nature of voxel-wise studies that are commonly reported in standard stereotaxic space (x, y, z) by pooling 3D coordinates from like studies, and providing the probability of an event occurring at each brain voxel. ALE implements algorithms that utilize a random-effects approach that minimizes within-experiment and within-groups effects (Eickhoff et al. 2012; Turkeltaub et al. 2012). Resultant ALE maps from the present study were thresholded using $p_{\text{cluster-corrected}} < 0.05$ (1000 permutations) and $p_{\text{pvoxel-level}} < 0.001$ (Eickhoff et al. 2016). Anatomical labels of convergent clusters were determined by the Talairach Daemon. To quantitatively test for co-activation and co-deactivation differences in the PCC, and the dPCC and vPCC subregions, we performed contrast analyses. Using GingerALE, we pooled the co-deactivation and co-activation ALE maps together and randomly divided them into 2 groups (of the same size as the original maps) 10,000 times to create a null-distribution, permitting subsequent statistical testing for differences in ALE scores between the two maps. Resultant ALE scores were tested against a null hypothesis at each voxel to produce a voxel-wise p value image, which was then converted to a z score map. We used a cluster-wise FWE-corrected p value of 0.001, which Kessler et al. (2017) validated as an effective method of cluster-wise thresholding, and a cluster threshold of 200 mm^3. Contrast analyses allow for a conservative quantitative assessment of shared and differential functional activity patterns in MACM datasets.

Behavioral and paradigm class analyses To better understand the cognitive and behavioral processes associated with regions specifically co-activated and co-deactivated with the PCC, we utilized the behavioral analysis and paradigm analysis plugins within Mango. These plugins allow for an automated regional behavioral analysis that uses the BrainMap® lexicon (www.brainmap.org/taxonomy/) of behavioral domains and paradigm classes (Lancaster et al. 2012). The behavioral analysis presents results for the five behavioral domains (Action, Cognition, Emotion, Interoception, and Perception) as well as sixty sub-domains and an associated z score where only z scores of 3.0 or higher are considered significant (corresponding to a $p < 0.05$ with Bonferroni correction for multiple comparisons) (Lancaster et al. 2012). Similarly, the paradigm analysis results are presented for the paradigm classes (i.e., experimental tasks) and use the same significance criteria. Behavioral and paradigm analyses were conducted on resultant contrast images from the PCC activation and deactivation MACM contrast analyses using ROI tools in Mango.

Ultra-high field magnetic resonance imaging methods

Resting state functional magnetic resonance imaging (rs-fMRI)

We performed ultra-high field (7T), high-resolution (i.e., submillimeter) rs-fMRI to characterize the functional connectivity of the PCC. Data were acquired on the Auburn University MRI Research Center (AUMRIRC) Siemens 7T MAGNETOM outfitted with a 32-channel head coil by Nova Medical (Wilmington, MA). Thirty-one healthy individuals (26 right-handed, 12 males/19 females, age: M ± SD = 21.13 ± 1.43 years old) provided informed consent and were scanned using an echo planar imaging (EPI) sequence, optimized in-house to reduce noise and artifacts typically seen in sub-cortical regions at high field strengths (37 slices acquired parallel to the AC-PC line, 0.85 mm × 0.85 mm × 1.5 mm voxels, TR/TE: 3000/28 ms, 70° flip angle, base/phase resolution 234/100, A > P phase encode direction, iPAT GRAPPA acceleration factor = 3, interleaved acquisition, 100 time points, total acquisition time 5:00). During the scan, participants were asked to rest with their eyes closed. A whole-brain high-resolution 3D image (256 slices, 0.63 mm × 0.63 mm × 0.60 mm, TR/TE: 2200/2.8, 7° flip angle, base/phase resolution 384/100%, collected in an ascending fashion, acquisition time = 14:06) was acquired for registration purposes. Data were analyzed in SPM8 (Ashburner 2012) and the 'conn' connectivity toolbox (version 17a) (Whitfield-Gabrieli and Nieto-Castanon 2012) using standard rs-fMRI pre-processing steps (i.e., brain extraction, slice timing correction, Gaussian smoothing

(5 mm FWHM), band-pass filtering (0.008–0.09), regression of motion, physiological artifacts, white matter, and CSF [using CompCor methods (Behzadi et al. 2007)], removal of aberrant motion volumes from analyses (i.e., "scrubbing"), registration to anatomical space, and normalization to MNI standard space). The PCC ROI was defined as a 'seed' and functional connectivity was determined across the entire brain. Seed-to-voxel connectivity maps were thresholded at $p_{\text{FDR-corrected}} < 0.001$ at the voxel-level and $p_{\text{FWE-corrected}} < 0.001$ at the cluster-level (two-tailed).

Results

Meta-analytic connectivity modeling

Co-activation

We found a number of regions co-activated with the PCC (Table 1). Specifically, we found evidence for strong co-activation in prefrontal regions (i.e., bilateral inferior and middle frontal gyri, left medial frontal gyrus, and left precentral gyrus) and key limbic structures (i.e., left anterior cingulate, left midcingulate gyrus, bilateral amygdala, bilateral insula, and left parahippocampal gyrus). In addition, we found support for co-activation with attentional and spatial networks inclusive of parietal regions (i.e., left inferior parietal lobule, bilateral precuneus, left superior parietal lobule). Finally, co-activation was also noted among temporal regions (i.e., left middle temporal gyrus) as well as sub-cortical structures (i.e., bilateral globus pallidus, and thalamus). These data demonstrate the extensive number of regions and diversity of regions associated with the PCC when in a functionally activated state.

Co-deactivation

Fewer brain regions were shown to co-deactivate with the PCC (Table 2). Notably, this result may be due to poor reporting of deactivation studies as well as fewer foci in deactivation studies. However, interestingly, limbic regions such as the bilateral anterior cingulate, midcingulate gyrus, and left amygdala were identified as functionally co-deactivated during a deactivated state of the PCC.

Quantitative contrast analysis

We found support for both convergent and divergent regions when conducting a contrast analysis of the two individual meta-analyses (PCC activation versus PCC deactivation) (Table 3 and Fig. 2). Generally, the meta-analytic functional pattern related to PCC co-activation was more extensive compared to the functional pattern of PCC co-deactivation. Areas of convergence between maps of co-activation and co-deactivation of the PCC include the left medial frontal gyrus, left midcingulate gyrus, left amygdala, and left anterior cingulate. These structures may be associated with mechanisms for increased and decreased concomitant co-activation or co-deactivation with the PCC.

PCC co-activation > PCC co-deactivation Bilateral inferior frontal gyri, medial frontal gyri, and left middle frontal gyrus as well as sub-cortical regions such as the bilateral claustrum, right putamen, right medial globus pallidus, and left thalamus were uniquely co-activated to the PCC during activated compared to deactivated states. Additionally, bilateral midcingulate gyri, extending from supplementary to pre-supplementary motor cortices, and portions of the left inferior parietal lobule and right superior parietal lobule were also identified as co-activated.

PCC co-deactivation > PCC co-activation Frontal regions associated with greater co-deactivation of the PCC compared to PCC co-activation include bilateral frontal gyri and the left paracentral lobule. In addition, limbic regions such as portions of the left and right midcingulate gyri, left anterior cingulate, and left parahippocampal gyrus showed greater co-deactivation with the PCC. The left precuneus was also co-deactivated with PCC deactivation.

Behavioral and paradigm analyses For the ROI inclusive of regions specifically co-activated with the PCC, the behavioral analysis indicated significant behavioral prevalence associated with Cognition, Emotion, Perception, and Action domains (Table 4). Statistically significant sub-domains for Cognition included Language (Semantics; Speech; Phonology; Orthography; Syntax), Attention, Reasoning, Memory (Explicit; Working), Social Cognition, and Music. Sub-domains for Emotion included Positive (Reward/Gain; Happiness), and Negative (Sadness; Disgust). Sub-domains for Action included Inhibition and Execution (Speech). Last, sub-domains for Perception included Somesthesis (Pain; Unspecified) and Vision (Shape). The most significant behavioral domain was Cognition with sub-domain Attention ($z = 10.46$). The paradigm analysis listing indicated 19 tasks as being significantly related to co-activation of the PCC (for complete listing see Table 5). The three most significant paradigm classes were Reward ($z = 8.28$), Semantic Monitor/Discrimination ($z = 7.54$), and Go/No–Go ($z = 5.74$). For the ROI inclusive of regions specifically co-deactivated with the PCC, neither the behavioral nor paradigm analyses yielded significantly associated behavioral domains or significantly associated paradigm class with the functional pattern specific to co-deactivation of the PCC.

Table 1 Regions of co-activation with PCC activation

ALE	*x*	*y*	*z*	Lobe	Region	BA
0.073	– 48	28	2	Frontal	Left inferior frontal gyrus	13
0.113	– 2	54	– 8		Left medial frontal gyrus	
0.109	– 2	60	– 2		Left medial frontal gyrus	10
0.100	– 2	62	8		Left medial frontal gyrus	10
0.070	– 4	56	24		Left medial frontal gyrus	9
0.062	2	4	60		Left medial frontal gyrus	6
0.073	– 46	28	18		Left middle frontal gyrus	46
0.067	– 38	14	46		Left middle frontal gyrus	6
0.059	– 28	20	52		Left middle frontal gyrus	6
0.057	– 36	8	58		Left middle frontal gyrus	6
0.080	– 48	10	36		Left precentral gyrus	6
0.073	50	16	28		Right inferior frontal gyrus	9
0.063	52	30	– 6		Right inferior frontal gyrus	45
0.063	46	12	44		Right middle frontal gyrus	6
0.116	0	48	– 10	Limbic	Left anterior cingulate	32
0.066	– 2	42	4		Left anterior cingulate	32
0.299	2	– 28	32		Left cingulate gyrus	31
0.274	– 2	– 48	30		Left cingulate gyrus	31
0.100	0	24	30		Left cingulate gyrus	32
0.094	– 2	22	42		Left cingulate gyrus	32
0.090	0	32	26		Left cingulate gyrus	32
0.092	– 24	– 8	– 18		Left amygdala	
0.059	– 24	– 22	– 18		Left parahippocampal gyrus	28
0.072	24	– 4	– 18		Right amygdala	
0.077	8	– 46	6		Right posterior cingulate	29
0.063	– 8	– 22	– 6	Midbrain	Left red nucleus	
0.055	2	– 28	– 4		Left red nucleus	
0.069	– 42	– 52	50	Parietal	Left inferior parietal lobule	40
0.054	– 40	– 64	48		Left inferior parietal lobule	39
0.078	– 6	– 72	42		Left precuneus	7
0.079	– 30	– 62	50		Left superior parietal lobule	7
0.066	12	– 72	42		Right precuneus	7
0.123	– 34	20	0	Sub-cortical	Left insula	13
0.091	– 48	16	– 6		Left insula	13
0.087	– 12	8	– 2		Left lateral globus pallidus	
0.082	– 14	4	8		Left putamen	
0.114	– 10	– 14	8		Left thalamus–medial dorsal nucleus	
0.053	36	16	– 16		Right extra-nuclear	13
0.107	50	16	– 4		Right insula	13
0.101	36	22	– 2		Right insula	
0.094	18	6	– 2		Right lateral globus pallidus	
0.093	10	– 12	10		Right thalamus–medial dorsal nucleus	
0.121	– 48	– 64	28	Temporal	Left middle temporal gyrus	39
0.091	– 44	– 72	36		Left middle temporal gyrus	39

Table 2 Regions of co-deactivation with PCC deactivation

ALE	*x*	*y*	*z*	Lobe	Region	BA
0.048	– 2	58	8	Frontal	Left medial frontal gyrus	9
0.035	– 4	52	– 6	Limbic	Left anterior cingulate	32
0.076	0	– 48	30		Left cingulate gyrus	31
0.033	0	– 24	32		Left cingulate gyrus	23
0.025	– 26	– 10	– 18		Left parahippocampal gyrus–amygdala	
0.030	– 24	– 6	– 26		Left uncus–amygdala	
0.028	2	32	– 14		Right anterior cingulate	24
0.025	6	50	– 14		Right anterior cingulate	32
0.022	0	36	– 4		Right anterior cingulate	
0.050	4	– 32	42		Right cingulate gyrus	31
0.028	52	– 68	18	Temporal	Right middle temporal gyrus	39
0.023	46	– 70	28		Right middle temporal gyrus	39

Exploratory meta-analytic connectivity modeling—dPCC and vPCC

Co-activation

We found a number of regions co-activated with either the dPCC or vPCC (Table 6). Regions found to be co-activated with the dPCC included the left medial frontal gyrus, right middle frontal gyrus, left midcingulate and posterior cingulate gyri, and the left inferior parietal lobule. In addition, sub-cortical structures, such as the left insula and bilateral claustrum, co-activated with the dPCC. For the vPCC, regions of co-activation included the bilateral medial frontal gyri, right posterior cingulate, left lingual gyrus, left precuneus and cuneus as well as the left middle temporal and right inferior temporal gyri.

Co-deactivation

Fewer brain regions were shown to be co-deactivated with either the dPCC or vPCC (Table 6). Regions showing co-deactivation with the dPCC included bilateral midcingulate gyri, right posterior cingulate and left caudate. Regions showing co-deactivation with the vPCC included the left midcingulate gyrus and right posterior cingulate, bilateral precuneus, and the right middle temporal gyrus.

Quantitative contrast analysis

We found support for convergent and divergent regions of co-activation and co-deactivation when conducting contrast analyses. We conducted four contrast analyses: dPCC co-activation versus dPCC co-deactivation, vPCC co-activation versus vPCC co-deactivation, dPCC co-activation versus vPCC co-activation, dPCC co-deactivation versus vPCC co-deactivation (Table 7, Fig. 3). Regions of convergence for dPCC co-activation and dPCC co-deactivation included bilateral midcingulate gyri and the right posterior cingulate. For the vPCC co-activation and co-deactivation contrast, regions of convergence included bilateral precuneus and the left midcingulate gyrus. The dPCC co-activation and vPCC co-activation contrast yielded regions of convergence including the left medial frontal gyrus and the left posterior cingulate. For the dPCC co-deactivations versus vPCC co-deactivations contrasts, regions of convergence included the right midcingulate and posterior cingulate gyri. Given the low number of deactivation papers, the following results should be interpreted with caution. In particular, warning messages appeared stating it was unlikely to have enough statistical power to show significant differences for two of the four contrasts, dPCC co-activation versus dPCC co-deactivation and dPCC co-deactivation versus vPCC co-deactivation.

d(v)PCC Co-activation > d(v)PCC Co-deactivation, d(v)PCC Co-(de)activation > v(d)PCC Co-(de)activation The contrast of dPCC co-activation versus dPCC co-deactivation did not yield any significant regions of divergence. Similarly, the contrast for vPCC co-activation versus vPCC co-deactivation did not yield significant regions of divergence. In contrasting dPCC co-activation with vPCC co-activation, the right posterior cingulate (BA23) and left inferior parietal lobule emerged as regions uniquely co-activated with the dPCC and the right posterior cingulate (BA 31) and right precuneus emerged as regions uniquely co-activated with the vPCC. In contrasting dPCC co-deactivation with vPCC co-deactivation, the left posterior cingulate and left midcingulate gyrus were shown to co-deactivate uniquely with the dPCC. No regions emerged as uniquely co-deactivated with the vPCC.

Behavioral and paradigm analyses

For the ROI inclusive of regions specifically co-activated with the dPCC, neither the behavioral analysis listing nor the paradigm analysis yielded behavioral domains or paradigm classes significantly related to the dPCC co-activation profile.

Table 3 Statistically significant differences between functional activity patterns associated with co-activation of the PCC and co-deactivation of the PCC as determined by MACM contrast analyses, thresholded at an FDR-corrected $p < 0.05$

z score	*x*	*y*	*z*	Lobe	Region	BA
Co-activation > co-deactivation						
3.719	42.4	21.2	– 5.3	Frontal	Right inferior frontal gyrus	47
3.719	– 45.4	5.2	34.4		Left inferior frontal gyrus	9
3.090	– 46	27	6		Left inferior frontal gyrus	13
3.719	3.2	17.4	49		Right medial frontal gyrus	32
3.239	– 4	30	46		Left medial frontal gyrus	8
3.353	– 42	8	52		Left middle frontal gyrus	6
3.540	32	18	– 6	Sub-cortical	Right claustrum	
3.719	– 32.8	19.2	– 2.3		Left claustrum	
3.353	– 30	18	5		Left claustrum	
3.540	– 43.4	18.8	– 1.6		Left insula	13
3.156	28	0	– 2		Right putamen	
3.719	20.5	3.5	– 1.4		Right putamen	
3.540	12	2	0		Right medial globus pallidus	
3.719	– 9.1	– 11.4	– 0.3		Left thalamus	
3.540	– 7.7	– 13.3	– 2		Left thalamus	
3.156	32	– 2	– 6		Right putamen	
3.090	26	– 2	0		Right putamen	
3.090	24	0	0		Right putamen	
3.540	4	22.4	45.8	Limbic	Right cingulate gyrus	32
3.353	– 3	15	24		Left cingulate gyrus	24
3.239	– 6	14	28		Left cingulate gyrus	24
3.090	– 2	16	32		Left cingulate gyrus	24
3.156	– 6	30	42		Left cingulate gyrus	32
3.156	– 43	– 52	56	Parietal	Left inferior parietal lobule	40
3.156	32	– 56	50		Right superior parietal lobule	7
3.239	– 3.3	– 24.7	– 5.3	Midbrain	Red nucleus	
Co-deactivation > co-activation						
3.719	8.7	59.3	1.3	Frontal	Right medial frontal gyrus	10
3.719	10	53.3	– 15.3		Right medial frontal gyrus	10
3.353	4	34	– 20		Right medial frontal gyrus	11
3.540	– 0.7	57.3	7.3		Left medial frontal gyrus	10
3.156	0	56	10		Left medial frontal gyrus	9
3.090	– 6	– 20	58		Left medial frontal gyrus	6
3.540	– 6	– 24	54		Left paracentral lobule	6
3.719	8	– 32	46.8	Limbic	Right cingulate gyrus	31
3.090	6	– 40	42		Right cingulate gyrus	31
3.719	0.2	29.8	– 13.8		Left anterior cingulate	24
3.540	2	– 42	44		Left cingulate gyrus	31
3.719	– 23	– 5.8	– 28.6		Left parahippocampal gyrus	35
3.719	2	– 47.3	41.3	Parietal	Left precuneus	31

Coordinates are reported in MNI space

Similarly, for the ROI inclusive of regions specifically co-activated with vPCC, neither the behavioral nor paradigm class analyses yielded behavioral domains or paradigm classes significantly associated with the vPCC co-activation profile. In addition, no significant results emerged from the behavioral and paradigm analyses involving the ROI inclusive of regions specifically co-deactivated with the dPCC.

Resting state functional connectivity

Resting state functional connectivity analyses using the PCC as the seed resulted in widespread whole-brain activation. Despite demonstrating a similar pattern of connectivity to the activation-based MACM, a few notable exceptions emerged (Figs. 4, 5). Convergent patterns of resting state functional

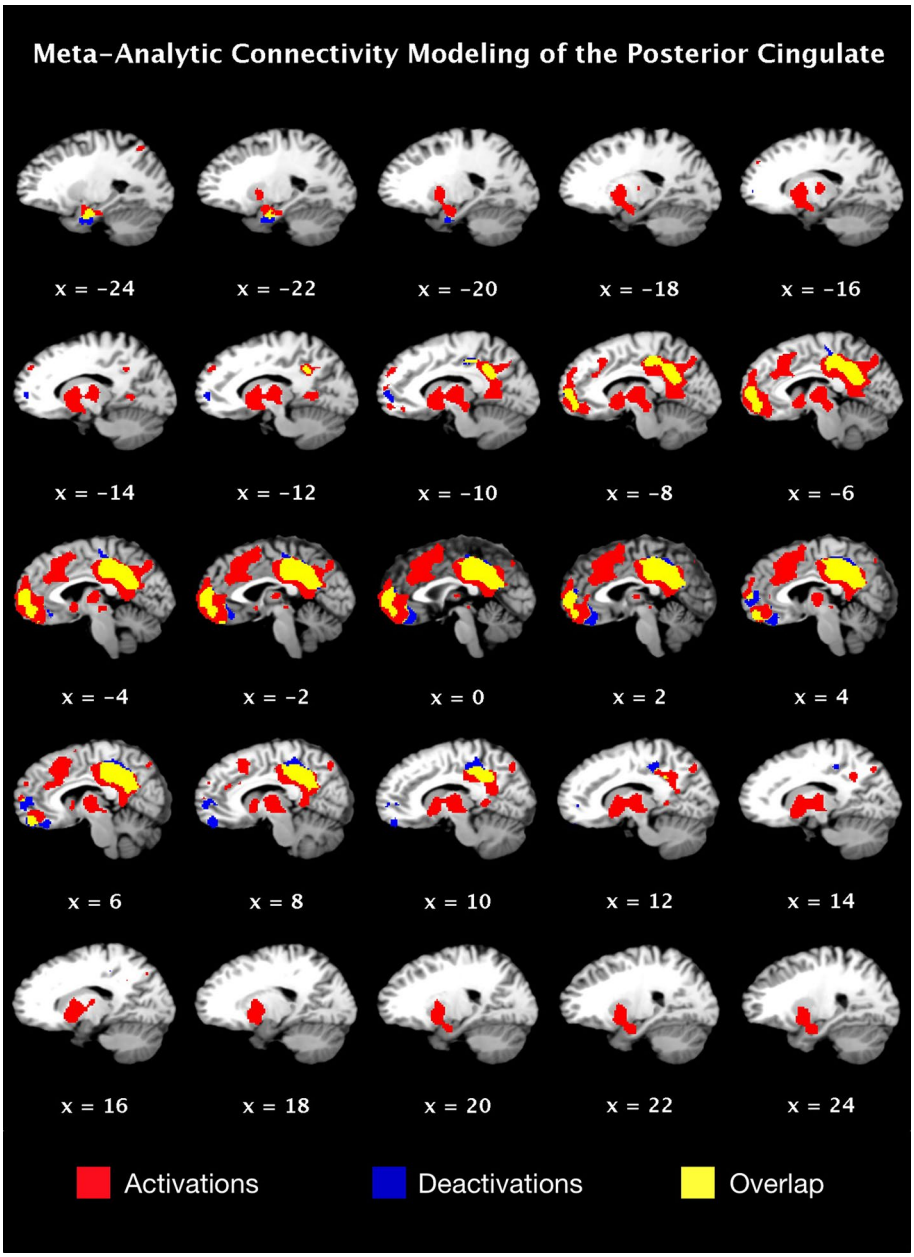

Fig. 2 Meta-analytic connectivity modeling of the PCC with overlays of the ALE maps for PCC co-activation and PCC co-deactivation MACMs and the qualitative overlap between the two MACMs. ALE maps were individually thresholded using $p_{\text{cluster-corrected}} < 0.05$ (1000 permutations) and $p_{\text{pvoxel-level}} < 0.001$

connectivity with co-activation were identified with the anterior cingulate, medial frontal gyrus, left parahippocampus, left culmen, portions of the left and right thalamus, the left middle/superior temporal gyri, and the left inferior parietal lobe (please see Supplemental Information for a full table of local maxima). Resting state connectivity also demonstrated differential patterns of functional connectivity in bilateral superior parietal regions, as well as right inferior parietal regions and superior temporal regions. We also noted bilateral pulvinar and superior frontal gyri connectivity specific to resting state data. In addition, similar to the pattern displayed when comparing co-activation with co-deactivation, we saw co-activation in sub-cortical regions such as the bilateral claustrum, right putamen, right medial globus pallidus, and left thalamus as well as bilateral midcingulate gyri extending from supplementary to pre-supplementary motor cortices, compared to resting state connectivity.

Discussion

Given the roles of the PCC, inclusive of involvement in opposing networks, we sought to identify a comprehensive functional model of the PCC (including exploratory analyses of dorsal and ventral subregions) during task-based activated and deactivated states as well as resting state using advanced meta-analytic techniques combined with rs-fMRI. MACM results provided evidence for regions of convergence for both PCC activation and deactivation as

Table 4 Significant results for the behavioral analysis of the ROI inclusive of regions co-activated with the PCC

Category	Domain	*z* score
Attention	Cognition	10.462
Language (Semantics)	Cognition	8.879
Reasoning	Cognition	8.289
Positive (Reward/Gain)	Emotion	7.822
Memory (Explicit)	Cognition	7.727
Language (Speech)	Cognition	7.089
Memory (Working)	Cognition	5.920
Inhibition	Action	5.761
Language (Phonology)	Cognition	5.738
Somesthesis (Pain)	Perception	4.876
Somesthesis (Unspecified)	Perception	4.093
Language (Orthography)	Cognition	4.063
Negative (Sadness)	Emotion	3.805
Social Cognition	Cognition	3.587
Positive (Happiness)	Emotion	3.577
Negative (Disgust)	Emotion	3.523
Music	Cognition	3.507
Execution (Speech)	Action	3.353
Vision (Shape)	Perception	3.312
Language (Syntax)	Cognition	3.001

Table 5 SignifIcant results of the paradigm analysis for the ROI inclusive of regions co-activated with the PCC

Category	*z* score
Reward	8.276
Semantic monitor/discrimination	7.535
Go/No-Go	5.739
Finger tapping/button press	5.671
n-back	5.287
Cued explicit recognition/recall	5.242
Pain monitor/discrimination	5.024
Phonological discrimination	4.966
Stroop-Color	4.246
Face monitor/discrimination	4.098
Paired associate recall	3.923
Word generation (Covert)	3.863
Film viewing	3.656
Counting/calculation	3.655
Delayed match to sample	3.583
Emotion induction	3.325
Orthographic discrimination	3.314
Encoding	3.312
Episodic recall	3.234

well as divergent regions specific to either PCC activation or PCC deactivation. Similarly, conducting co-activation and co-deactivation-based MACMs on dorsal and ventral subregions of the PCC resulted in both divergent and convergent functional activity. To further explore divergent patterns of functional activity, we employed behavioral and paradigm analyses which characterized psychological phenomena consistently associated with regional-specific activation or deactivation across archived neuroimaging experiments. Resting-state functional connectivity analyses demonstrated widespread agreement regarding those brain regions showing co-activation with the PCC via meta-analytic modeling; however, we observed additional regions that were not convergent with results from the original meta-analyses. These complementary results support the notion that there are dissociable functional patterns of the PCC associated with task- and resting-states. Taken together, these analyses highlight the diverse neurofunctional repertoire of the human PCC, and provide additional insight into its dynamic functional activity patterns.

MACM analyses

PCC

The activation based MACM results closely mimicked regions of the DMN. For example, regions co-activated specifically with activation of the PCC, such as the left and right inferior frontal gyri, left and right medial frontal gyri, left and right parietal lobules, left and right claustrum, left insula, left thalamus, and left and right cingulate gyri have been noted as being representative of the DMN (Raichle et al. 2001). However, we also found co-activation in the right putamen and right medial globus pallidus, and red nucleus, which can be attributed to the integral role the cingulate gyrus plays in the limbic system for emotion processing (Hadland et al. 2003) and memory (Kozlovskiy et al. 2012). These co-activations of regions in the parietal memory network (Gilmore et al. 2015) further highlight the PCC's role in memory of novel versus familiar stimuli. In addition, a mind-wandering state, (i.e., when the DMN is active), characterized by thought processes such as thinking about others, thinking of one's self, remembering the past, and envisioning the future (Andrews-Hanna 2012) explains the additional co-activation found in limbic, affective processing, and memory regions. As such, the activation MACM supported studies indicating the pivotal role the structure plays in the DMN as well as previous studies implicating the PCC in multiple neural networks.

The deactivation based MACM results revealed fewer regions that co-deactivate with the PCC compared to the number of regions that co-activate. Co-deactivated regions were largely involved in attention networks (i.e., right and left medial frontal gyri areas, portions of the cingulate, and left precuneus), suggesting a switch between DMN activities and directed attention (Leech et al. 2012). Interestingly, the

Table 6 Regions of co-activation and co-deactivation for dorsal and ventral subregions of the PCC

ALE	*x*	*y*	*z*	Lobe	Region	BA
dPCC co-activation						
0.016	0	60	– 4	Frontal	Left medial frontal gyrus	10
0.035	– 2	52	8		Left medial frontal gyrus	9
0.025	50	26	16		Right middle frontal gyrus	46
0.023	44	38	22		Right middle frontal gyrus	9
0.028	48	14	30		Right middle frontal gyrus	9
0.030	0	24	28	Limbic	Left cingulate gyrus	32
0.081	0	– 34	26		Left posterior cingulate	23
0.027	– 34	– 50	50	Parietal	Left inferior parietal lobule	40
0.024	– 32	16	– 8	Sub-cortical	Left claustrum	
0.034	– 34	20	0		Left insula	13
0.030	– 50	14	– 2		Left insula	13
0.030	36	16	– 4		Right claustrum	
vPCC co-activation						
0.030	– 10	54	0	Frontal	Left medial frontal gyrus	10
0.031	0	54	– 8		Right medial frontal gyrus	
0.121	4	– 56	24	Limbic	Right posterior cingulate	23
0.025	– 10	– 58	8	Occipital	Left lingual gyrus	18
0.028	– 16	– 64	22		Left precuneus	31
0.046	26	– 68	22		Right cuneus	18
0.046	– 48	– 64	24	Temporal	Left middle temporal gyrus	39
0.034	– 44	– 70	36		Left middle temporal gyrus	39
0.041	62	– 10	– 22		Right inferior temporal gyrus	21
dPCC co-deactivation						
0.011	0	– 36	28	Limbic	Left cingulate gyrus	31
0.017	6	– 46	30		Right cingulate gyrus	31
0.010	10	– 34	28		Right posterior cingulate	23
0.013	– 6	8	0	Sub-cortical	Left caudate	
vPCC co-deactivation						
0.028	– 4	– 56	30	Limbic	Left cingulate gyrus	31
0.013	10	– 38	30		Right posterior cingulate	23
0.018	– 8	– 66	24	Occipital	Left precuneus	31
0.040	4	– 62	22		Right precuneus	23
0.012	10	– 54	40	Parietal	Right precuneus	7
0.018	48	– 64	20	Temporal	Right middle temporal gyrus	39

Table 7 Statistically significant differences between functional activity patterns associated with co-activation and co-deactivation of dorsal and ventral subregions of the PCC as determined by MACM contrast analyses, thresholded at an FDR-corrected $p < 0.05$

z score	*x*	*y*	*z*	Lobe	Region	BA
dPCC co-activation > vPCC co-activation						
3.291	2.9	– 36.4	26.5	Limbic	Right posterior cingulate	23
3.291	– 35.9	– 50.1	45.8	Parietal	Left inferior parietal lobule	40
vPCC co-activation > dPCC co-activation						
3.090	30.5	– 63.5	19.5	Limbic	Right posterior cingulate	31
3.291	3.3	– 62.4	21.8	Occipital	Right precuneus	23
dPCC co-deactivation > vPCC co-deactivation						
3.291	– 0.7	– 32.7	29	Limbic	Left cingulate gyrus	23
3.090	– 4	– 36	26		Left posterior cingulate	23

Coordinates are reported in MNI space

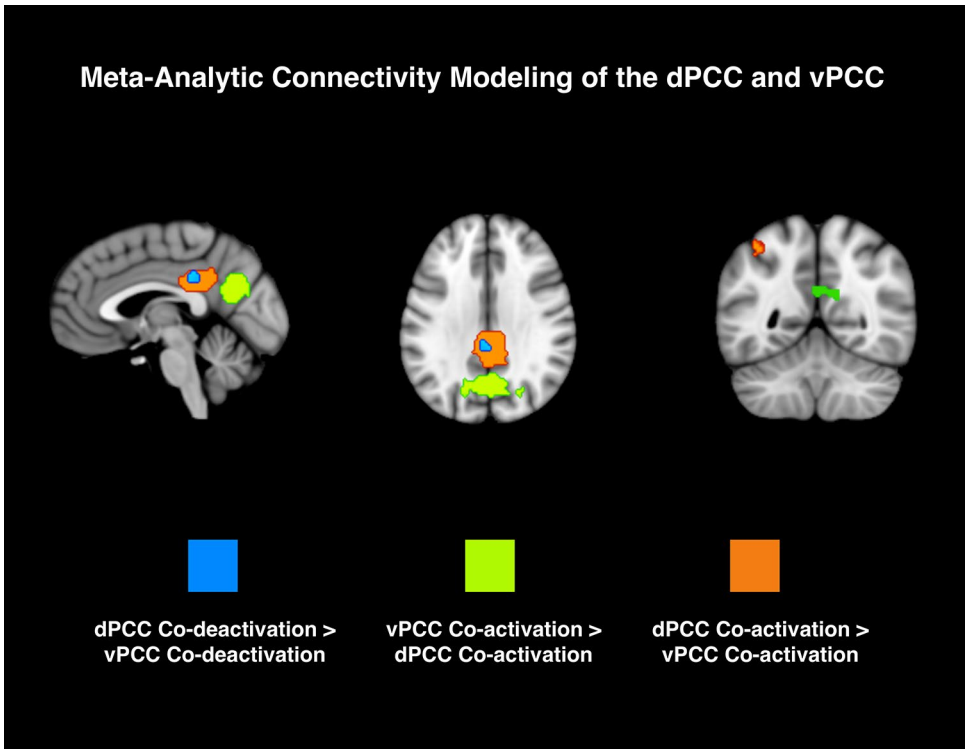

Fig. 3 Meta-analytic connectivity modeling of the dPCC and vPCC with overlays of the ALE maps for dPCC co-activation and vPCC co-activation and co-deactivation contrast MACMs. ALE maps were individually thresholded using $p_{\text{cluster-corrected}} < 0.05$ (1000 permutations) and $p_{\text{pvoxel-level}} < 0.001$

portions of the cingulate that co-deactivate with the PCC appear to be in the cingulate sulcus/premotor area suggesting a possible link to behavior control. The unique co-deactivation pattern included structures not limited to the DMN and, thus, further supports evidence for the PCC's involvement in multiple neural networks (Leech and Sharp 2014).

Converging regions of functional activity and differences between PCC co-activation and PCC co-deactivation were identified in our quantitative contrast analyses. Regions associated with PCC co-activation greater than co-deactivation consisted of DMN and cognitive processing regions. These results align with the assertion that the PCC may play a key role in regulating the focus of attention and is additionally supported because the majority of contributing studies for both the deactivation and activation MACMs were cognition-related, followed by perception-related. Regions with PCC co-deactivation greater than co-activation included a smaller subgroup of frontal and limbic regions associated with emotion processing and attentional control such as the bilateral cingulate and frontal gyri. This pattern of co-deactivation may be indicative of regions displaying inhibitory inputs into the PCC leading to the decrease of BOLD signal (Frankenstein et al. 2003). In addition, these findings can be further explained by cognitive processes such as the temporal bounding that left frontal regions have with working memory as compared to right frontal regions which contributes to cognitive processes that support adaptive decision-making and goal-directed behavior (Barbey et al. 2009, 2014). Similarly, the right amygdala has been proposed to act in a rapid, automatic manner in initiating an arousal response to the presentation of external stimulation (Gläscher et al. 2003; Hardee et al. 2008). It may also be that the right amygdala is more involved in global processing while the left is more involved in local, more detailed processing (Cahill 2006). Our results for the deactivation MACM display, importantly, that the PCC is more than just an area that deactivates along with the DMN in response to attentionally demanding tasks. Future research exploring lateralized aspects related to the co-deactivation findings may be profitable for gaining a deeper understanding of attentional control as it pertains to an efficient use of the left and right hemispheres.

According to the behavioral analyses, regions co-activated with the PCC were found to be engaged in the behavioral domains of Cognition, Emotion, Action, and Perception with Cognition being the most significant and most predominant. These results highlight the vital role of activation of the PCC in cognitive processes, in particular processes involving attention, language, and memory. As evidence, the paradigm analyses showed 19 paradigm classes associated with PCC activation, and roughly 13 of those 19 are tasks geared to measure attention, language, and memory, such as Go/No-Go, Semantic Monitor/Discrimination, and n-back as examples. The second most predominant behavioral domain shown to be associated with PCC activation was Emotion and included both positive emotion and negative emotion categories indicating that activation of the PCC related to emotion is not valence specific. This suggests that not only

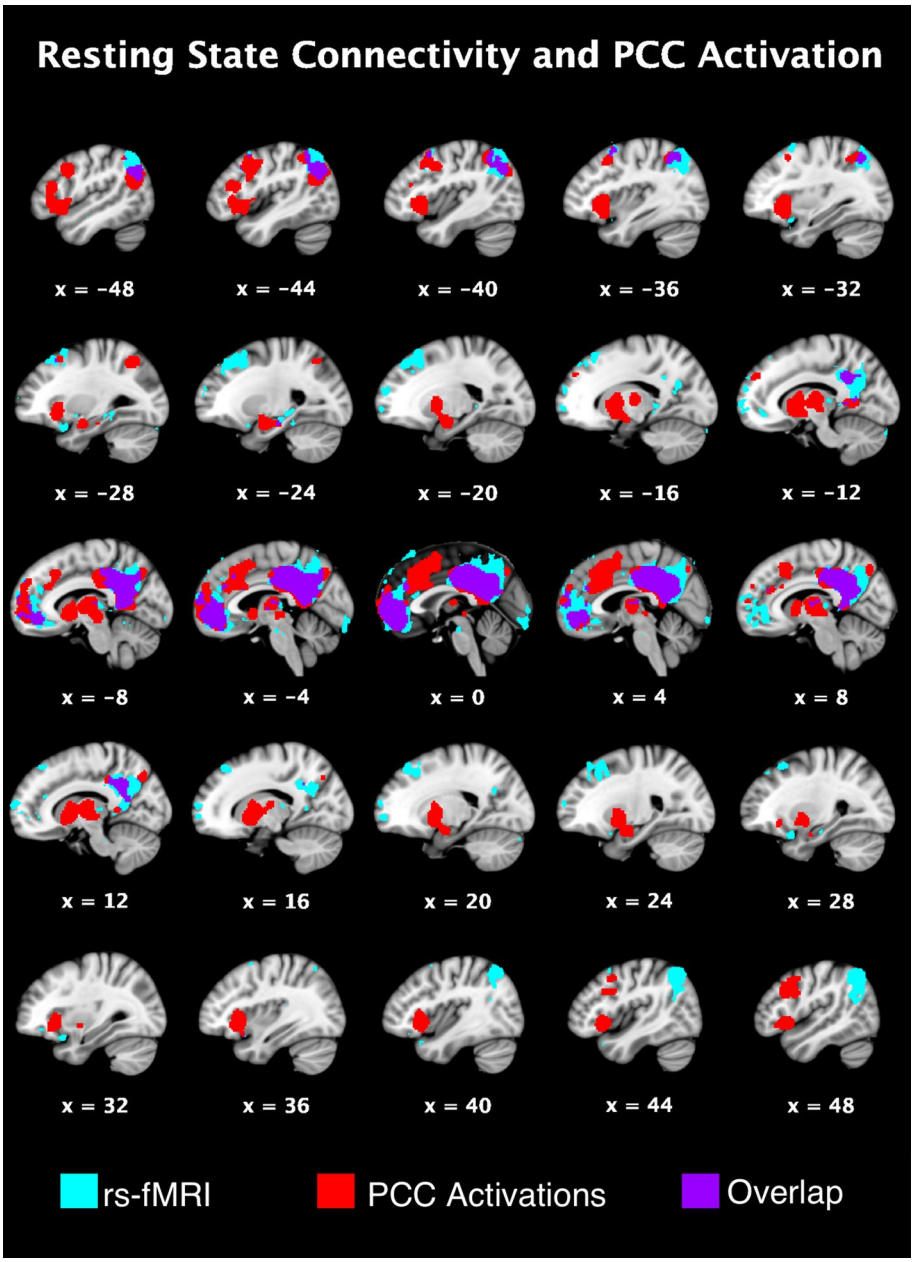

Fig. 4 Qualitative comparison of rs-fMRI and MACM activations for the PCC ROI. ALE maps were thresholded using $p_{\text{cluster-corrected}} < 0.05$ (1000 permutations) and $p_{\text{pvoxel-level}} < 0.001$. Rs-fMRI seed-to-voxel connectivity maps were thresholded at $p_{\text{FDR-corrected}} < 0.001$ at the voxel-level and $p_{\text{FWE-corrected}} < 0.001$ at the cluster-level (two-tailed)

is the PCC a hub for a number of cognitive processes, but it may also be a hub for emotion processing. The paradigm analyses partially corroborate this notion with significant paradigms classes of Reward and Emotion Induction shown to be associated with PCC activation. The behavioral and paradigm analyses provide a more specific understanding of the functional differences associated with PCC activation and highlight promising avenues for future research. In particular, the lack of significance in the behavioral and paradigm analyses for regions co-deactivated with the PCC, warrants further research to better understand the differences in the activation and deactivation functional profiles of the human PCC.

dPCC and vPCC

To further explore the co-activation and co-deactivation pattern of the PCC, we conducted exploratory MACMs and quantitative contrast analyses on defined dorsal and ventral subregions of the PCC. In doing so, we found evidence for divergent and convergent functional activity with respect to dPCC and vPCC subregions. While we discuss these results in the following paragraphs, the results should be interpreted with caution due to few papers reporting deactivations which contributed to warnings regarding power associated with two of the contrast analyses.

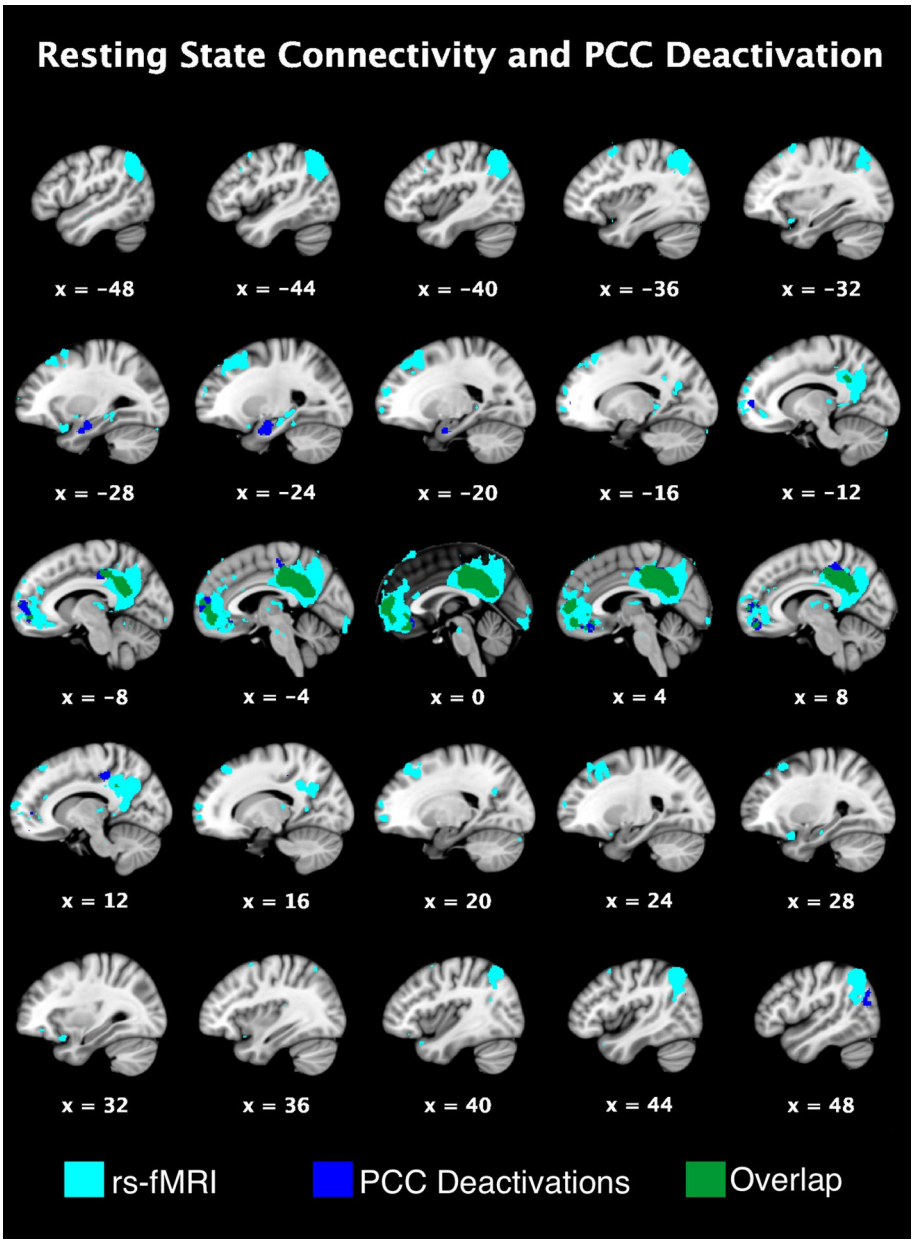

Fig. 5 Qualitative comparison of rs-fMRI and MACM deactivations for the PCC ROI. ALE maps were thresholded using $p_{\text{cluster-corrected}} < 0.05$ (1000 permutations) and $p_{\text{pvoxel-level}} < 0.001$. Rs-fMRI seed-to-voxel connectivity maps were thresholded at $p_{\text{FDR-corrected}} < 0.001$ at the voxel-level and $p_{\text{FWE-corrected}} < 0.001$ at the cluster-level (two-tailed)

For the activation-based MACM of the dPCC, co-activation appeared in regions associated with executive functioning (Talati and Hirsch 2005), consciousness (Crick and Koch 2005), and internal awareness of bodily sensations (i.e., medial and middle frontal gyri, claustrum, and insula; Craig 2009). These results suggest divergence from the proposed visuospatial functional specialization of the dPCC (Vogt et al. 2006). To that end, the quantitative contrast analyses demonstrated unique co-activation of the left inferior parietal lobule which has been shown to be associated with emotion perception (Radua et al. 2010), further suggesting the dPCC's involvement in functions beyond spatial processing. Despite having low power for the dPCC and vPCC activation and deactivation comparisons, these diverging results showing the dPCC's involvement in functions beyond spatial processing warrant further investigation. For the activation-based MACM of the vPCC, co-activation appeared in regions such as left precuneus, cuneus, and left middle and right inferior temporal gyri, that support the postulated role of the vPCC in self-reflection and self-awareness (Vogt et al. 2006) as well as self-referential processing (Yu et al. 2011) and facial appraisals (Bzdok et al. 2015) along with the co-activation with bilateral medial frontal gyri. Moreover, the quantitative contrast analyses showed unique co-activation in a portion of the right posterior cingulate and precuneus when compared to the dPCC co-activation, further corroborating the role of the vPCC in aspects of internal mentation and imagery. Regions of convergence for co-activation

between the dPCC and vPCC included the left medial frontal gyrus and the left PCC suggesting that portions of the PCC itself serve as a hub along a dorsal–ventral gradient of functional activity (Vogt et al. 2006) and implicating the medial frontal gyrus as an aid in attention shifting among executive functions related to perception, consciousness, and internal mentation.

For both the deactivation-based MACMs, the data demonstrated fewer regions of co-deactivation compared the regions of co-activation. Notably, the dPCC showed co-deactivation with the caudate, a structure associated with reward processing, suggesting that the dPCC deactivates during tasks associated with reward. For the vPCC, regions of co-deactivation included the precuneus, which has been show to be involved in episodic memory (Kjaer et al. 2002), self-reflections (Lou et al. 2004), and aspects of consciousness (Vogt and Laureys 2005), as well as other regions of perceptual processing such as the right middle temporal gyrus and cingulate gyrus. Co-deactivation with these regions suggests a task-negative association of the dPCC for tasks involving reward processing and a task-negative association for the vPCC for tasks requiring internal, self-relevant processing. The relative lack of results for quantitative contrast analyses indicate that statistical differences co-deactivation profiles of the dPCC and vPCC are more difficult to detect with notably fewer papers and experiments reporting deactivation. Converging regions of co-deactivation between the dPCC and vPCC included the right cingulate and posterior cingulate gyri, indicating that portions of the PCC may serve as a functional hub for both activation and deactivation.

PCC state-independent convergence

Regions of convergence for both PCC activation and PCC deactivation included a key region of the DMN, left medial frontal gyrus, displaying the significant functional connectivity relationship between the PCC and the left medial frontal gyrus, regardless of state of activation. Activation in the left medial frontal gyrus is unsurprising as the region has been implicated in lower level processing streams (Talati and Hirsch 2005). Other regions of convergences such as the left midcingulate gyrus, amygdala, and anterior cingulate emphasize the potential role these regions play in internal mentation given their co-activation and co-deactivation with the PCC. In addition, these regions have been implicated to involve emotion processing that requires both internal and externally directed thought with the left amygdala being shown to be associated with fearful stimuli (Vytal and Hamann 2010), the anterior cingulate with emotion awareness (Bush et al. 2000) and the midcingulate gyrus with rewarded behaviors in decision making (Vogt 2016). The areas of convergence between activation and deactivation of the PCC show regions connected to the PCC that are more variably activated or deactivated displaying that the deactivation pattern of the PCC has a dynamic functional profile in which different levels of deactivation may be manifest. Taken together, these data provide evidence for distinct functional patterns during activated and deactivated states, and suggest a differentiation between involvement in cognition (i.e., co-activated patterns) and attentional/affective processes (i.e., co-deactivated). Further exploration of specific attentional/affective task paradigms for the deactivated state of the PCC beyond the realm of the BrainMap® database, which is largely comprised of studies in cognition, is necessary to further elucidate the causes of distinct patterns of connectivity during activated and deactivated states.

Resting state PCC connectivity

Our study used high field submillimeter rs-fMRI to examine PCC resting state functional connectivity. Given that rs-fMRI elicits DMN activation, we expected to find consistent patterns of co-activation with DMN hubs. However, we also identified an extensive resting state functional connectivity pattern well beyond structures associated with the DMN, in line with other research (Leech and Sharp 2014; Vogt et al. 2006). These results bolster the notion that the PCC plays a versatile role not limited to the DMN (Leech et al. 2012; Leech and Sharp 2014), and that activation of this structure appears to "prime" several other structures involved in multiple networks including cognitive (i.e., medial prefrontal gyri), emotional (i.e., cingulate gyri), and attentional (i.e., frontal gyri) processes. These results demonstrate the need for studies interrogating the PCC via multiple behavioral domain tasks and suggest that focusing solely on the DMN may not be ideal in studies interested in the PCC. Our findings may be limited to a lack of record of what type of thought processing (internal versus external) participants were exhibiting during resting state data collection, another important factor to consider in future studies.

Finding widespread resting state functional connectivity of the PCC that converges and diverges from PCC co-activation and co-deactivation highlights the variable nature of resting state functional connectivity (Buckner et al. 2013) and supports evidence of an "intrinsic" functional brain organization that is present across various task types, including rest (Cole et al. 2014). To that end, functional regions active during rest may involve task-dependent co-activation or co-deactivation of regions depending on the internal and explicit mentation of the participants (Campbell and Schacter 2017) such as the case of our PCC MACM and rs-fMRI data. In addition, rs-fMRI has been suggested to be conceptually viewed as another task state that involves transient functional activity patterns inclusive of regions that are either anatomically or functionally coupled (Buckner et al. 2013; Krienen et al. 2014). Moreover, functional

activity patterns in resting state fMRI can be used to predict individual differences during task-based fMRI (Tavor et al. 2016) furthering the benefit of investigating functional activity patterns of versatile regions, such as the PCC, using multiple data types (i.e., meta-analytic activation and deactivation, and rs-fMRI).

Limitations of the present study include those that are shared among meta-analysis based methods. Limitations specific to the use of MACM and ALE are varying results influenced by user-specified criteria within the ALE program (i.e., family wise error, minimum cluster size) and by the thresholding of the initial ROIs used for analysis. In the current study, our contrast results should be interpreted with caution due to the significantly greater number of experiments associated with activation of the PCC compared to deactivation of the PCC, particularly with respect to the MACMs on the dPCC and vPCC subregions. The difference in the number of papers for each meta-analysis highlights the need for more published papers representing deactivation of the PCC. Throughout much of the fMRI literature a publication bias exists for studies describing activation of various regions in the brain while leaving unreported those regions deactivated, perhaps due to a lack of understanding of the interpretations of deactivation or negative BOLD responses (Frankenstein et al. 2003; Hayes and Huxtable 2012). In addition, the current paper uses the term 'deactivation' based on its usage within the BrainMap database consisting of mostly experiments reporting subtraction contrasts; thus, equating deactivation in this case may not be associated with an actual decrease in BOLD signal. Despite this potential limitation, the current work still provides a basis, using meta-analytic data, to spur further experimental research on deactivation properties of the PCC. In addition, while rs-fMRI data is common and a reasonable approach to functional connectivity during the non-task state, both the rs-fMRI and MACM data lack task-specific information. This is beneficial for identifying models of functional activity that are non-task specific. However, given that the PCC plays a role in multiple neural networks, it may be advantageous to investigate task specificity related to activation or deactivation of the human PCC and to further specify in terms of dorsal and ventral subregions of the PCC. Last, the construction our PCC ROI was done based on probability which may have impacted our results warranting future studies to investigate deactivation profiles based other atlas definitions and subregions of the PCC.

In the current paper, we used a combination of big data resources (i.e., the BrainMap® database) as well as ultra-high field, high resolution rs-fMRI to unpack the functional profiles of PCC activation versus PCC deactivation and then compared to resting state connectivity. In addition, we conducted behavioral and paradigm analyses to further explore resultant differences in PCC activation versus deactivation functioning. We also explored activation and deactivation profiles of dorsal and ventral subregions of the PCC. To our knowledge, this is the first study aimed at developing a functional model of the human PCC that compares task-based activation, task-based deactivation, and task-independent resting state. Furthermore, our data provide a more detailed account of the functional profile of the human PCC in healthy individuals, using completely noninvasive methodology. This study contributes to the understanding of the human PCC via a multi-state assessment and highlights the need for more research, in the PCC and more generally, regarding deactivations in functional activity.

Our results are consistent in showing the PCC as a central hub within the DMN (Leech et al. 2012). However, given that we found regions of divergence in connectivity patterns between activation and deactivation of the PCC and similarly with respect to dPCC and vPCC subregions, our results provide evidence for more diverse involvement of the PCC (Leech et al. 2012; Leech and Sharp 2014). Developing such models of functional connectivity during activation and deactivation may improve our understanding of disease states in which differential connectivity between the PCC and other brain regions is noted. Given this, future research should examine MACM based functional models using structural equation modeling (SEM) of healthy and diseased populations with known deficits in the PCC based on both PCC activation and deactivation as well as effective connectivity patterns between groups. This would further contribute to the clinical implications of aberrant PCC functioning depending on either an activated and deactivated state.

Acknowledgements A Collaborative Use Agreement exists between JLR and the BrainMap® Database.

Compliance with ethical standards

Conflict of interest All authors report having no financial, personal, or organizational conflict of interest with the work outlined in this manuscript.

Human and animal rights The work outlined in this manuscript does not involve the use of human subjects as defined by the Institutional Review Board and no informed consent was necessary.

References

Acikalin MY, Gorgolewski KJ, Poldrack RA (2017) A coordinate-based meta-analysis of overlaps in regional specialization and functional connectivity across subjective value and default mode networks. Front Neurosci 11:1–11. https://doi.org/10.3389/fnins.2017.00001

Andrews-Hanna JR (2012) The brain's default network and its adaptive role in internal mentation. The Neuroscientist 18(3):251–270. https://doi.org/10.1177/1073858411403316

Ashburner J (2012) SPM: a history. NeuroImage 62:791–800
Bai F, Watson DR, Yu H, Shi Y, Yuan Y, Zhang Z (2009) Abnormal resting-state functional connectivity of posterior cingulate cortex in amnestic type mild cognitive impairment. Brain Res 1302:167–174. https://doi.org/10.1016/j.brainres.2009.09.028
Barbey AK, Krueger F, Grafman J (2009) Structured event complexes in the medial prefrontal cortex support counterfactual representations for future planning. Philos Trans R Soc B Biol Sci 364(1521):1291–1300. https://doi.org/10.1098/rstb.2008.0315
Barbey AK, Colom R, Paul EJ, Grafman J (2014) Architecture of fluid intelligence and working memory revealed by lesion mapping. Brain Struct Funct 219(2):485–494. https://doi.org/10.1007/s00429-013-0512-z
Behzadi Y, Restom K, Liau J, Liu TT (2007) A component based noise correction method (CompCor) for BOLD and perfusion based fMRI. NeuroImage 37(1):90–101. https://doi.org/10.1016/J.NEUROIMAGE.2007.04.042
Buckner RL, Andrews-Hanna JR, Schacter DL (2008) The brain's default network: anatomy, function, and relevance to disease. Ann NY Acad Sci 1124:1–38. https://doi.org/10.1196/annals.1440.011
Buckner RL, Krienen FM, Yeo BTT (2013) Opportunities and limitations of intrinsic functional connectivity MRI. Nat Neurosci 16(7):832–837. https://doi.org/10.1038/nn.3423
Bush G, Luu P, Posner MI (2000) Cognitive and emotional influences in anterior cingulate cortex. Trends Cognit Sci 4(6):215–222. https://doi.org/10.1016/S1364-6613(00)01483-2
Bzdok D, Heeger A, Langner R, Laird AR, Fox PT, Palomero-Gallagher N, Eickhoff SB (2015) Subspecialization in the human posterior medial cortex. NeuroImage 106:55–71. https://doi.org/10.1016/j.neuroimage.2014.11.009
Cahill L (2006) Sex-related influences on the neurobiology of emotionally influenced memory. Ann NY Acad Sci 985(1):163–173. https://doi.org/10.1111/j.1749-6632.2003.tb07080.x
Campbell KL, Schacter DL (2017) Ageing and the resting state: is cognition obsolete? Lang Cognit Neurosci 32(6):661–668. https://doi.org/10.1080/23273798.2016.1227858
Cha J, Jo HJ, Gibson WS, Lee JM (2017) Functional organization of the human posterior cingulate cortex, revealed by multiple connectivity-based parcellation methods. Hum Brain Mapp 38(6):2808–2818. https://doi.org/10.1002/hbm.23570
Cherkassky VL, Kana RK, Keller TA, Just MA (2006) Functional connectivity in a baseline resting-state network in autism. NeuroReport 17(16):1687–1690. https://doi.org/10.1097/01.wnr.0000239956.45448.4c
Cole MW, Bassett DS, Power JD, Braver TS, Petersen SE (2014) Intrinsic and task-evoked network architectures of the human brain. Neuron 83(1):238–251. https://doi.org/10.1016/J.NEURON.2014.05.014
Craig AD (2009) How do you feel–now? The anterior insula and human awareness. Nat Rev Neurosci 10(1):59–70. https://doi.org/10.1038/nrn2555
Crick FC, Koch C (2005) What is the function of the claustrum? Philos Trans R Soc Lond B Biol Sci 360(1458):1271–1279. https://doi.org/10.1098/rstb.2005.1661
Eickhoff S, Laird A, Grefkes C, Wang LE, Zilles K, Fox PT (2009) Coordinate-based ALE meta-analysis of neuroimaging data: a random-effects approach based on empirical estimates of spatial uncertainty. Hum Brain Mapp 30(9):2907–2926. https://doi.org/10.1002/hbm.20718.Coordinate-based
Eickhoff SB, Bzdok D, Laird AR, Kurth F, Fox PT (2012) Activation likelihood estimation meta-analysis revisited. NeuroImage 59(3):2349–2361. https://doi.org/10.1016/j.neuroimage.2011.09.017
Eickhoff SB, Laird AR, Fox PM, Lancaster JL, Fox PT (2016) Implementation errors in the GingerALE software: description and recommendations. Human Brain Mapp 15:8. https://doi.org/10.1002/hbm.23342
Fox PT, Laird AR, Fox SP, Fox PM, Uecker AM, Crank M, Lancaster JL (2005) BrainMap taxonomy of experimental design: description and evaluation. IHuman Brain Mapp 25:185–198. https://doi.org/10.1002/hbm.20141
Frankenstein U, Wennerberg A, Richter W, Bernstein C, Morden D, Rémy F, Mcintyre M (2003) Activation and deactivation in blood oxygenation level dependent functional magnetic resonance imaging. Concepts Magn Reson 16A(1):63–70. https://doi.org/10.1002/cmr.a.10054
Fransson P, Marrelec G (2008) The precuneus/posterior cingulate cortex plays a pivotal role in the default mode network: evidence from a partial correlation network analysis. Neuroimage 42:1178–1184. https://doi.org/10.1016/j.neuroimage.2008.05.059
Gilmore AW, Nelson SM, McDermott KB (2015) A parietal memory network revealed by multiple MRI methods. Trends Cognit Sci 19(9):534–543. https://doi.org/10.1016/j.tics.2015.07.004
Gläscher J, Adolphs R, Gläscher J, Adolphs R, Glascher J, Adolphs R (2003) Processing of the arousal of subliminal and supraliminal emotional stimuli by the human amygdala. J Neurosci 23(32):10274–10282. https://doi.org/10.1523/JNEUROSCI.23-32-10274.2003
Hadland K, Rushworth MF, Gaffan D, Passingham R (2003) The effect of cingulate lesions on social behaviour and emotion. Neuropsychologia 41(8):919–931. https://doi.org/10.1016/S0028-3932(02)00325-1
Hale JR, Brookes MJ, Hall EL, Zumer JM, Stevenson CM, Francis ST, Morris PG (2010) Comparison of functional connectivity in default mode and sensorimotor networks at 3 and 7T. Magn Reson Mater Phys 23:339–349. https://doi.org/10.1007/s10334-010-0220-0
Hardee JE, Thompson JC, Puce A (2008) The left amygdala knows fear: laterality in the amygdala response to fearful eyes. Soc Cognit Affect Neurosci 3(1):47–54. https://doi.org/10.1093/scan/nsn001
Hayes DJ, Huxtable AG (2012) Interpreting deactivations in neuroimaging. Front Psychol 3:27. https://doi.org/10.3389/fpsyg.2012.00027
Kessler D, Angstadt M, Sripada CS (2017) Reevaluating "cluster failure" in fMRI using nonparametric control of the false discovery rate. Proc Natl Acad Sci 114(17):E3372–E3373. https://doi.org/10.1073/pnas.1614502114
Kjaer TW, Nowak M, Lou HC (2002) Reflective self-awareness and conscious states: pet evidence for a common midline parietofrontal core. NeuroImage 17(2):1080–1086. https://doi.org/10.1006/NIMG.2002.1230
Krienen FM, Yeo BTT, Buckner RL (2014) Reconfigurable task-dependent functional coupling modes cluster around a core functional architecture. Philos Trans R Soc B Bio Sci 369(1653):20130526. https://doi.org/10.1098/rstb.2013.0526
Kozlovskiy SA, Nikonova EY, Pyasik MM, Velichkovsky BM (2012) The cingulate cortex and human memory processes. Psychol Russia 5:231
Laird AR, Fox PM, Price CJ, Glahn DC, Uecker AM, Lancaster JL, Fox PT (2005a) ALE meta-analysis: controlling the false discovery rate and performing statistical contrasts. Hum Brain Mapp 25:155–164. https://doi.org/10.1002/hbm.20136
Laird AR, Lancaster JL, Fox PT (2005b) BrainMap: the social evolution of a human brain mapping database. Neuroinformatics. https://doi.org/10.1385/NI:3:1:065
Lancaster JL, Laird AR, Eickhoff SB, Martinez MJ, Fox PM, Fox PT (2012) Automated regional behavioral analysis for human brain imaging. Front Neuroinform 6:23. https://doi.org/10.3389/fninf.2012.00023

Leech R, Sharp DJ (2014) The role of the posterior cingulate cortex in cognition and disease. Brain 137(1):12–32. https://doi.org/10.1093/brain/awt162

Leech R, Kamourieh S, Beckmann CF, Sharp DJ (2011) Fractionating the default mode network: distinct contributions of the ventral and dorsal posterior cingulate cortex to cognitive control. J Neurosci 31(9):3217–3224. https://doi.org/10.1523/JNEUROSCI.5626-10.2011

Leech R, Braga R, Sharp DJ (2012) Echoes of the brain within the posterior cingulate. Cortex 32(1):215–222. https://doi.org/10.1523/JNEUROSCI.3689-11.2012

Liang M, Zhou Y, Jiang T, Liu Z, Tian L, Liu H, Hao Y (2006) Widespread functional disconnectivity in schizophrenia with resting-state functional magnetic resonance imaging. NeuroReport 17(2):209–213. https://doi.org/10.1097/01.wnr.0000198434.06518.b8

Lord AR, Li M, Demenescu LR, van den Meer J, Borchardt V, Krause AL, Walter M (2017) Richness in functional connectivity depends on the neuronal integrity within the posterior cingulate cortex. Front Neurosci 11:184. https://doi.org/10.3389/fnins.2017.00184

Lou HC, Luber B, Crupain M, Keenan JP, Nowak M, Kjaer TW, Lisanby SH (2004) Parietal cortex and representation of the mental Self. Proc Natl Acad Sci USA 101(17):6827–6832. https://doi.org/10.1073/pnas.0400049101

Maddock RJ, Garrett AS, Buonocore MH (2001) Remembering familiar people: the posterior cingulate cortex and autobiographical memory retrieval. Neuroscience 104(3):667–676. https://doi.org/10.1016/S0306-4522(01)00108-7

Maddock RJ, Garrett AS, Buonocore MH (2003) Posterior cingulate cortex activation by emotional words: fMRI evidence from a valence decision task. Hum Brain Mapp 18(1):30–41. https://doi.org/10.1002/hbm.10075

Miller CH, Hamilton JP, Sacchet MD, Gotlib IH (2015) Meta-analysis of functional neuroimaging of major depressive disorder in youth. JAMA Psychiatry 72(10):1045–1053. https://doi.org/10.1001/jamapsychiatry.2015.1376

Nakao T, Radua J, Rubia K, Mataix-Cols D (2011) Gray matter volume abnormalities in ADHD: voxel-based meta-analysis exploring the effects of age and stimulant medication. Am J Psychiatry 168(11):1154–1163. https://doi.org/10.1176/appi.ajp.2011.11020281

Nowogrodzki A (2018) The world's strongest MRI machines are pushing human imaging to ne limits. Nature 563:24–26. https://doi.org/10.1038/d41586-018-07182-7

Radua J, Philips ML, Russell T, Lawrence N, Marshall N, Kalidindi Sl, David AS (2010) Neural response to specific components of fearful faces in healthy and schizophrenic adults. Neuroimage 49(1):939–946. https://doi.org/10.1016/j.neuroimage.2009.08.030

Raichle ME, Macleod AM, Snyder AZ, Powers WJ, Gusnard DA, Shulman GL (2001) A default mode of brain function. Proc Natl Acad Sci 98(2):676–682

Robinson JL, Laird AR, Glahn DC, Lovallo WR, Fox PT (2009) Metaanalytic connectivity modeling: delineating the functional connectivity of the human amygdala. Hum Brain Mapp. https://doi.org/10.1002/hbm.20854

Robinson JL, Erath SA, Kana RK, El-Sheikh M (2018) Neurophysiological differences in the adolescent brain following a single night of restricted sleep—a 7T fMRI study. Dev Cognit Neurosci 31:1–10. https://doi.org/10.1016/J.DCN.2018.03.012

Sämann PG, Wehrle R, Hoehn D, Spoormaker VI, Peters H, Tully C, Czisch M (2011) Development of the brain's default mode network from wakefulness to slow wave sleep. Cereb Cortex 21(9):2082–2093. https://doi.org/10.1093/cercor/bhq295

Singh KD, Fawcett IP (2008) Transient and linearly graded deactivation of the human default-mode network by a visual detection task. NeuroImage 41(1):100–112. https://doi.org/10.1016/j.neuroimage.2008.01.051

Talati A, Hirsch J (2005) Functional specialization within the medial frontal gyrus for perceptual go/no-go decisions based on related information: an fMRI study. J Cognit Neurosci 17(7):981–993. https://doi.org/10.1162/0898929054475226

Tavor I, Parker Jones O, Mars RB, Smith SM, Behrens TE, Jbabdi S (2016) Task-free MRI predicts individual differences in brain activity during task performance. Science 352(6282):216–220. https://doi.org/10.1126/science.aad8127

Turkeltaub PE, Eickhoff SB, Laird AR, Fox M, Wiener M, Fox P (2012) Minimizing within-experiment and within-group effects in activation likelihood estimation meta-analyses. Hum Brain Mapp 33(1):1–13. https://doi.org/10.1002/hbm.21186

van den Heuvel MP, Sporns O (2011) Rich-club organization of the human connectome. J Neurosci 31(44):15775–15786. https://doi.org/10.1523/JNEUROSCI.3539-11.2011

Vogt BA (2016) Midcingulate cortex: structure, connections, homologies, functions and diseases. J Chem Neuroanat 74:28–46. https://doi.org/10.1016/j.jchemneu.2016.01.010

Vogt BA, Laureys S (2005) Posterior cingulate, precuneal and retrosplenial cortices: cytology and components of the neural network correlates of consciousness. Prog Brain Res 150:205–217. https://doi.org/10.1016/S0079-6123(05)50015-3

Vogt BA, Vogt L, Laureys S (2006) Cytology and functionally correlated circuits of human posterior cingulate areas. Neuroimage 29:452–466. https://doi.org/10.1016/j.neuroimage.2005.07.048

Vytal K, Hamann S (2010) Neuroimaging support for discrete neural correlates of basic emotions: a voxel-based meta-analysis. Journal of Cogniti Neurosci 22(12):2864–2885. https://doi.org/10.1162/jocn.2009.21366

Whitfield-Gabrieli S, Nieto-Castanon A (2012) Conn: a functional connectivity toolbox for correlated and anticorrelated brain networks. Brain Connect 2:125–141

Yu C, Zhou Y, Liu Y, Jiang T, Dong H, Zhang Y, Walter M (2011) NeuroImage functional segregation of the human cingulate cortex is con firmed by functional connectivity based neuroanatomical parcellation. NeuroImage 54(4):2571–2581. https://doi.org/10.1016/j.neuroimage.2010.11.018

Zhu X, Wang X, Xiao J, Liao J, Zhong M, Wang W, Yao S (2012) Evidence of a dissociation pattern in resting-state default mode network connectivity in first-episode, treatment-naive major depression patients. Biol Psychiat 71(7):611–617. https://doi.org/10.1016/j.biopsych.2011.10.035